Geomechanics and Engineering, *Vol. 43, No. 1 (2025) 27-39*
https://doi.org/10.12989/gae.2025.43.1.027

Long-term durability of foamed concrete filler in highway engineering

Long Chen[1a], Yi Zhu[1b], Desheng Li*[1], Lunyang Zhao[2], Yonghui Chen[3] and Ming Huang[4]

[1]*College of Civil and Transportation Engineering, Hohai Univ., Nanjing, Jiangsu 210098, China*
[2]*School of Civil Engineering and Transportation, South China Univ. of Tech., Guangzhou, Guangdong 510641, China*
[3]*Suzhou Research Inst. of Hohai Univ., Suzhou, Jiangsu 215004, China*
[4]*The Fourth Construction Co., Ltd of China Railway Construction Engineering Group, Shanghai 201306, China*

(*Received July 21, 2024, Revised September 23, 2025, Accepted September 25, 2025*)

Abstract. In highway engineering, foamed concrete used for subgrade filler is typically influenced by external environmental factors such as freeze-thaw cycles and vehicle loads. This study conducts freeze-thaw cycle tests, load cycle tests, and coupling (freeze-thaw-load) cycle tests under the designed wet density to simulate the field environment of highway engineering and examine the strength variation of foamed concrete under different conditions. Additionally, the pore structure and freezing damage mechanism of foamed concrete were analyzed using SEM. The results indicate that the strength loss of foamed concrete exceeds 20% after 100 freeze-thaw cycles. During the load cycle tests, the compressive strength of foamed concrete can be divided into three stages, corresponding to the development of micro-cracks in the material. In the coupled environment to simulate field conditions, the compressive strength of foamed concrete decreases rapidly to 0.96 MPa (20.66% loss) after the first 10 years, which followed by a slower decline (0.83 MPa in the 20th years and 0.78 MPa in the 40th years). SEM analysis shows that the internal damage caused by freeze–thaw cycles can be categorized into cavity failure and crack failure.

Keywords: coupling cycles; foamed concrete; freeze-thaw cycles; load cycles; SEM analysis

1. Introduction

Foamed concrete, also known as light porous concrete (Kilincarslan *et al*. 2018), is a lightweight cement-based material produced by incorporating prefabricated foam into fresh cement mortar (Raj *et al*. 2021), with the foam content accounting for at least 20% of the material's volume (Van Dijk 1991). As a typical cellular material, foamed concrete exhibits characteristics such as light weight, high strength, high compressibility, excellent flowability, ductility, thermal insulation performance, and energy absorption (Amran, *et al*. 2015). Moreover, owing to its exceptional properties including density adjustability, low raw material cost, environmental friendliness, and favorable construction performance, foamed concrete is widely used in construction projects and underground engineering (Kadela and Kozlowski 2016, Ramamurthy *et al*. 2009), including abutment backfilling (Zhang, *et al*. 2020), embankment widening (Shi, *et al*. 2020), slope protection (Amran *et al*. 2022), tunnel reserved deformation layers (Zhang *et al*. 2024), and arresting systems for runways and airfields (Steyn *et al*. 2016). Particularly, due to the necessity of construction on soft soil and loose soils (Arasan and Nasirpur 2015), the utilization of foamed concrete as fillers in subgrade engineering within soft soil areas has become more widespread in recent years. Numerous studies indicate that using foamed concrete can reduce additional stress on foundations, control subgrade settlement, and decrease pavement deflection (Kim *et al*. 2013, She *et al*. 2018, Zhang *et al*. 2023). The long-term physical and mechanical properties of foamed concrete have a substantial impact on the safety and quality of related engineering projects (Zhang *et al*. 2022). Given that cement concrete pavement highways typically have a service life exceeding 30 years (JTG B01-2014), improving the durability of foamed concrete to meet these longevity requirements is of utmost practical importance.

The freeze-thaw cycle is one of the most common natural physical processes in cold regions (Cheng *et al*. 2021). The phenomenon of freeze-thaw erosion is widespread in China, affecting an area of 1.27×10^7 km^2, constituting 13.36% of the total land area (Wei *et al*. 2012). In the cold climate of the northeastern region, up to 120 freeze-thaw cycles occur within a year (Li *et al*. 2000). The activities of freeze-thaw geology lead to various issues in road construction, including frost heave, thawing settlement, freeze-thaw weathering, and pavement cracks, ultimately causing damage to the subgrade structure (Wu *et al*. 2023). Consequently, it is imperative to consider the impact of freeze-thaw cycles on subgrade structures during road construction in China. Foamed concrete, a commonly employed subgrade filler, warrants investigation into its property changes under freeze-thaw cycles to enhance its long-term durability significantly. Tan *et al*. (2013) conducted indoor freeze-thaw cycle tests on foamed concrete across a temperature range of -40°C to 40°C. The findings indicate an exponential decrease in compressive

*Corresponding author, Ph.D. Candidate
E-mail: lidesheng@hhu.edu.cn
[a]Professor
E-mail: longchenhhu@163.com
[b]Ph.D. Candidate
E-mail: zhuyi01eric@163.com

ISSN: 2005-307X (Print), 2092-6219 (Online)

Table 1 Physical and mechanical properties of the cement

Specific surface area (m^2/kg)	Density (kg/m^3)	Normal Consistency (%)	Setting time (min)		Compressive strength (MPa)		Flexural strength (MPa)	
			Initial setting	Final setting	3 days	28 days	3 days	28 days
358	3100	28.5	203	250	27.4	45.0	5.9	7.7

Table 2 Chemical composition of the cement

Components	CaO	SiO_2	Al_2O_3	Fe_2O_3	MgO
Content/%	63.30	19.95	5.06	3.34	2.54

strength with an increasing number of freeze-thaw cycles, with a reduction of approximately 43% after 40 cycles. Cai *et al*. (2021) observed that the frost resistance of foamed concrete gradually improves with increasing wet density. Specifically, the dynamic elastic modulus of the sample with 279 kg/m^3 density lost 41.1% after 20 freeze-thaw cycles. Tikalsky *et al*. (2004) demonstrated that compressive strength, initial penetration depth, and water absorption significantly influence the frost resistance of light porous concrete. To enhance the frost resistance of foamed concrete, a common approach involves incorporating materials with superior frost resistance, such as graphene oxide (Wang *et al*. 2023), PET fibers (Tang *et al*. 2022), pozzolanic powder (Gong and Zhang 2019), phosphogypsum (Li *et al*. 2020), and magnesium oxychloride (Zhong *et al*. 2021). Nevertheless, this practice inevitably results in resource wastage and increased costs.

During the road service period, pavement structures are susceptible to fatigue, cracking, or uneven permanent deformation under long-term traffic loading, which significantly compromises the comfort and safety of road (Brown 1996, Chai and Miura 2002, Krechowiecki-Shaw *et al*. 2016). Under repeated loading, the residual stresses within the subgrade can accelerate the deformation of the road structures (Tang *et al*. 2018). Thus, when utilizing foamed concrete as the subgrade filler, it becomes imperative to assess changes in its strength and deformation properties induced by cyclic dynamic loading. The dynamic properties of foamed concrete correlate closely with both strain rate and density (Feng *et al*. 2020). Wu *et al*. (2022) investigated the dynamic response of foamed concrete used in subgrade fillers through staged cyclic loading tests, revealing that its dynamic strength is inferior to its static counterpart. This occurs because cyclic loading, despite maintaining a constant stress amplitude, elevates plastic strain, resulting in heightened structural and strength degradation of foamed concrete. Cai *et al*. (2021) examined the long-term dynamic performance of foamed concrete under cyclic loading through a series of dynamic triaxial tests. Test results indicate that the critical dynamic stress of foamed concrete (i.e., the amplitude of dynamic stress required to reach a certain failure standard under a certain number of load cycles) typically ranges from 0.2 to 0.3 times the unconfined compressive strength. Under cyclic stress levels below the critical dynamic stress, cumulative settlement remains relatively stable. Conversely, exceeding the critical dynamic stress leads to linear increases in cumulative deformation until abrupt failure occurs.

The above literature demonstrates that the mechanical properties of foamed concrete under single cycles with fewer repetitions have been well studied. However, highway fill materials are subjected to both cyclic freeze-thaw actions and dynamic loads (referred to as coupling cycles), which significantly impact the durability of foamed concrete. Previous studies have not adequately addressed the durability evolution of foamed concrete under coupling cycle conditions, nor have they proposed a laboratory-appropriate coupling cycle simulation method for highway engineering. Additionally, classifying the failure types of foamed concrete under freeze-thaw cycles based on the failure origin and degree is a novel approach. Therefore, freeze-thaw cycle tests, load cycle tests, and coupling cycle tests were conducted to simulate the field environment of highway engineering, and the corresponding strength change law of foamed concrete was determined. Finally, the freeze-thaw failure mechanism of foamed concrete subjected to freeze-thaw cycles was elucidated using SEM.

2. Materials and methods

2.1 Materials

The experiment used ordinary Portland cement (P.O.42.5) for its basic physical and mechanical properties, as outlined in Table 1. The compressive strength and flexural strength of the cement were measured in accordance with the Chinese standard GB/T 17671-2021. The major components of the cement obtained from X-ray fluorescence spectroscopy (XRF) are shown in Table 2, with CaO and SiO_2 comprising 63.30% and 19.95% of the mass, respectively. A protein-based anionic foaming agent was employed in the experiment, boasting a foaming rate of 800-1000 times, with a standard density ranging from 40-50 kg/m^3. Its mechanism is that protein molecules adsorb at the gas–liquid interface, reduce surface tension, and form a dense, elastic film, thereby generating and stabilizing a large number of uniform pores (Chandni and Anand 2018). This foaming agent is devoid of any pungent odor and poses no adverse effects on the environment. Distilled water was used in the experiment to avoid impurities that could interfere with the foaming process.

2.2 Specimen preparation

After the wet density and water-cement ratio of the foamed concrete are provided, the volume of foam, and the

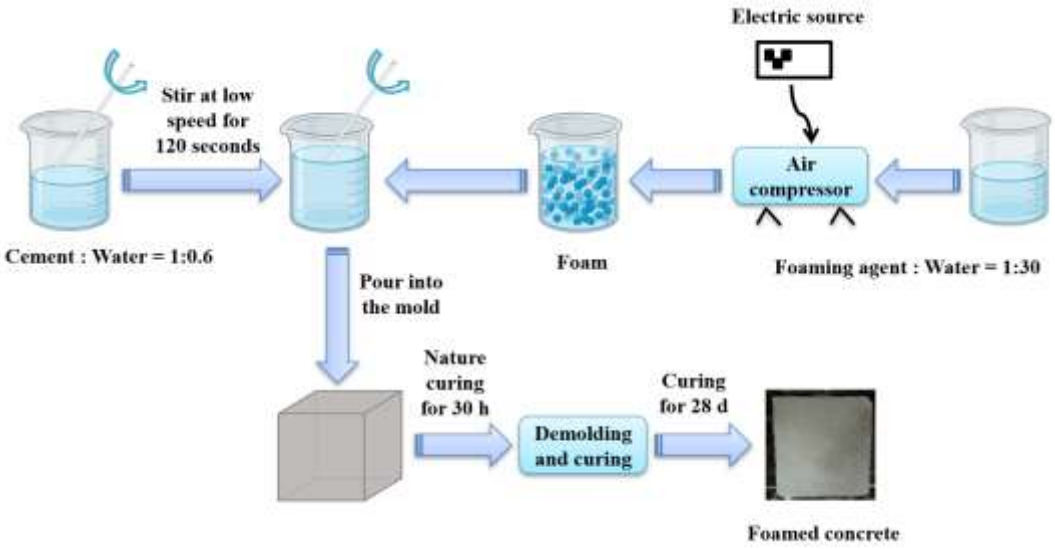

Fig. 1 Preparation process of specimens

Table 3 Mix proportions and measured characteristic values of the foamed concrete

Wet density (kg/m^3)	Dry density (kg/m^3)	Cement (kg/m^3)	Water (kg/m^3)	Foam (L)
600	570	350	210	677.1

weight of cement and water required to make the sample can be calculated (Jones and McCarthy 2005, Wei *et al*. 2013). The design mix proportions of foamed concrete are detailed in Table 3.

The sample size is 100 mm × 100 mm × 100 mm, and the preparation process is illustrated in Fig. 1 The physical foaming method, as specified in the Chinese standard JG/T 266-2011, was employed. A small air compressor serves as the foaming machine to blend the foaming agent and water in a 1:30 ratio, producing uniform and stable foam. Precise weighing to the nearest gram was conducted for the raw materials based on the calculated mixing ratio. Cement and water were mixed in a 1:0.6 ratio and stirred slowly for 2 minutes to form cement slurry. The pre-measured foam was then added and stirred for an additional 2 minutes until the mixture achieved uniformity.

To maintain the integrity of the test specimen, a steel plate was positioned at the bottom of the mold. The mold was meticulously cleaned and coated with the demolding agent, and a paper cover was used to seal the bottom demolding orifice to prevent any potential leakage. Initially, the slurry was poured into the mold halfway, followed by manual vibration of the mold. Subsequently, the slurry was poured to slightly exceed the mold's top edge, with further vibrating action applied until a smooth surface was achieved. While pouring the slurry, gently tap the mold to prevent the entrapment of large air bubbles inside the specimen. The filled mold was then left at room temperature for 30 hours before demolding and subsequent curing in a standard curing room for 28 days.

Table 4 Specimens for the freeze-thaw cycle test

Specimen	Number of cycles (times)	Corresponding service years
F1	1	0.2
F5	5	1
F10	10	2
F50	50	10
F100	100	20
F150	150	30
F200	200	40
F300	300	60

2.3 Test methods

2.3.1 Freeze-thaw cycle test

The annual average number of freeze-thaw cycles varies significantly across different regions of China: approximately 120 cycles in Northeast China, 84 cycles in North China, 118 cycles in Northwest China, and 18 cycles in Central China. East China, situated between North and Central China, experiences an annual average of 18 to 84 freeze-thaw cycles (Li, *et al*. 2000). According to the rapid freeze-thaw test method specified in ASTM C 666-97, one rapid freeze-thaw cycle conducted indoors is considered equivalent to 10 to 15 freeze-thaw cycles under natural conditions, with an average value of 12 cycles. In densely networked East China, where the road infrastructure is extensive, the average annual occurrence of freeze-thaw cycles is 60 times. This frequency serves as an example, equivalent to undergoing 5 cycles of rapid freeze-thaw in laboratory conditions. Given that the highway's design service life spans 50 years, the maximum number of rapid freeze-thaw cycles applied in the test is set at 300.

The test equipment utilized is the high and low temperature test chamber manufactured by HOONSHAN, with the test chamber measuring 400 mm × 400 mm × 500 mm. The test specimens were divided into 8 groups, each containing 3 specimens, to analyze the variation in strength of foamed concrete under different freeze-thaw cycles. The grouping of specimens is detailed in Table 4.

The freeze-thaw cycle test procedure was conducted in accordance with standards ASTM C 666-97 and JGJ-T341-2014. Initially, the specimens were dried to a constant mass in an electric blast drying oven, followed by immersion in a constant temperature tank at 20±5°C for 48 hours. Subsequently, the specimens underwent a freeze-thaw cycle, involving freezing at -20°C for 6 hours, followed by thawing at 20°C for 5 hours. This cycle was repeated until the desired number of freeze-thaw cycles was achieved. In the event of significant damage observed during visual inspection, the test was terminated. Upon reaching the specified number of cycles, the specimen was dried to a constant mass in an electric blast drying oven, and the compressive strength of the dried specimen was tested.

Following the freeze-thaw cycle, the unconfined compressive strength test was conducted in accordance with the testing requirements outlined in the JG/T 266-2011 standard. This test aimed to record the maximum load borne by the specimen and determine its compressive strength. The average compressive strength of each group of foamed concrete was calculated based on three specimens. The test utilized the WHY-10 electronic universal testing machine manufactured by Shanghai Hualong Testing Instrument Co., Ltd., with the descent rate of the universal testing machine set at 1.250 mm/min.

2.3.2 SEM analysis

The microstructure of foamed concrete samples was examined using a scanning electron microscope after undergoing freeze-thaw cycles. Initially, the samples were fractured, and blocks approximately 2 cm^3 in size were carefully selected and prepared from the central regions of these samples. The prepared samples were immersed in anhydrous ethanol until the hydration reaction ceased. Subsequently, the samples were removed from the ethanol, dried in an oven set at 50°C, and observed without polishing the surface, utilizing a natural section obtained by breaking the specimen in the middle. The Hitachi S-4800 scanning electron microscope, operating at an accelerated voltage of 5.0 kV, was employed for microscopic analysis.

2.3.3 Load cycle test

The cyclic loading induced by vehicular traffic leads to cumulative deformation and fatigue damage of foamed concrete, consequently diminishing its durability (Xu *et al*. 2018). Given that the stress-strain impact of vehicle loads on the pavement closely resembles a sine curve (Wu *et al*. 2022), the load waveform is configured as a sine wave in cyclic loading tests. According to the Chinese standard DB33/T 996-2015, foamed concrete utilized for roadbed filling should exhibit a 28-day unconfined compressive strength (f_c) of no less than 1.0 MPa; for embankment filling, the minimum 28-day unconfined compressive strength should be 0.6 MPa. During testing, the load cycle test limits for foamed concrete intended for roadbed filling range from 0.1 f_c to 0.66 f_c (equivalent to 0.1 MPa to 0.66 MPa), encompassing the lower and upper bounds, respectively (GB/T 50082-2009).

Table 5 Specimens for the load cycle test

Specimen	Number of cycles ($\times 10^4$ times)	Corresponding service years
L10	10	3.3
L40	40	13.3
L60	60	20
L80	80	26.7
L120	120	40
L180	180	60

The concrete compressive fatigue deformation test typically involves a load cycle number of 2 million times, roughly equivalent to the 50-year service cycle of heavily trafficked roads (GB/T 50082-2009). However, owing to the lower strength of foamed concrete, its load-bearing capacity is inferior to that of ordinary concrete. For this test, the maximum number of load cycles is set at 1.8 million, assuming that foamed concrete experiences approximately 30,000 load cycles per year.

The test utilized an SD300 electro-hydraulic servo static and dynamic universal testing machine. The cyclic loading and unloading frequency was set at 6 Hz (GB/T 50082-2009), with an amplitude of 2.8 kN (0.28 MPa) and an average of -3.8 kN (0.38 MPa). Test specimens were categorized into 6 groups, each containing 3 specimens, for the analysis of strength variation in foamed concrete under different load cycles. The specimen grouping is detailed in Table 5.

The load cycle test was conducted using an electro-hydraulic servo static and dynamic universal testing machine for the specified number of sine wave loadings. During the loading process, any cracks in the test specimen were promptly observed, and the number of cyclic loadings during crack development was recorded. Following the completion of the designated loading cycles, the unconfined compressive strength test was performed to measure the compressive strength of the test specimen after varying loading cycles.

2.3.4 Coupling cycle test

The subgrade is deemed the primary support structure, providing adequate strength and stability for the pavement to withstand vehicle loads (Cui *et al*. 2023, Lu *et al*. 2018). However, the behavior of the soil subgrade is complex and irregular against loads (Rahgooy *et al*. 2022). The coupling cycle test is designed to investigate the ability of subgrade structure to vehicle loads following a specified period of freeze-thaw erosion. Thus, in the coupling cycle test, the specimen undergoes the freeze-thaw cycle before the load cycle.

The specimen grouping for the coupling cycle test is presented in Table 6. Specimens are categorized into five groups, each comprising three specimens, to simulate the freeze-thaw and load cycles endured by foamed concrete

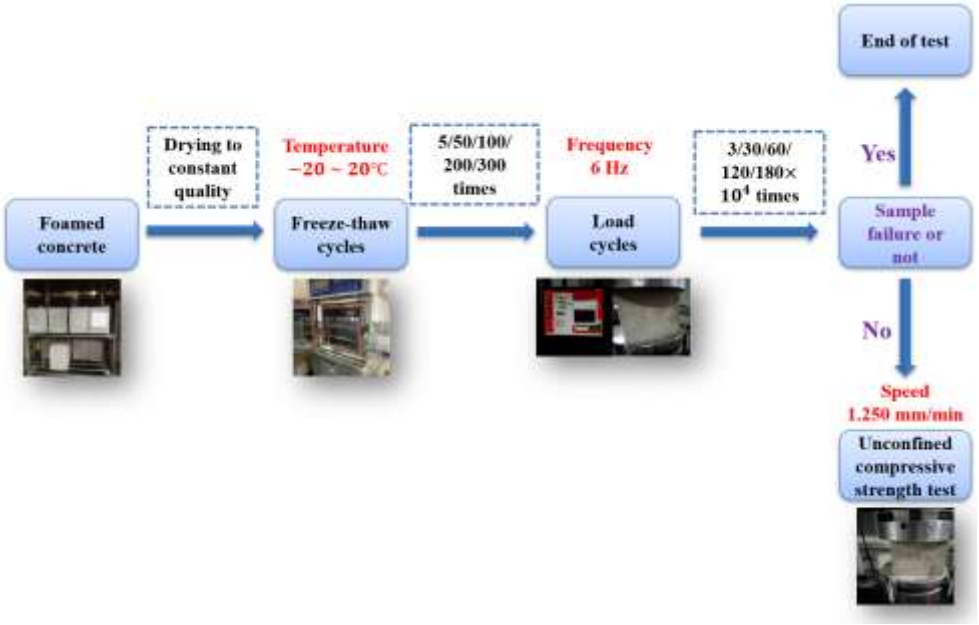

Fig. 2 Flow chart of the coupling cycle test

Table 6 Specimens for the coupling cycle test

Specimen	Freeze-thaw cycles (times) + load cycles (×10^4 times)	Corresponding service years
F5L3	5+3	1
F50L30	50+30	10
F100L60	100+60	20
F200L120	200+120	40
F300L180	300+180	60

over 60 years. As mentioned above, it is assumed that foamed concrete experiences approximately five freeze-thaw cycles and 30,000 load cycles annually.

The procedure for the coupling cycle test is depicted in Fig. 2. Initially, the cured specimens underwent freeze-thaw cycles, followed by cyclic loading and unloading upon completion of the freeze-thaw cycles. The test steps for both freeze-thaw cycles and load cycles were consistent with those described previously. Subsequently, the unconfined compressive strength test was conducted on the specimens that remained intact after the coupling cycle test, employing a loading rate of 1.250 mm/min.

3. Results and discussion

3.1 Freeze-thaw cycles

The compressive strength loss rate serves as an indicator of the extent of damage inflicted on foamed concrete by freeze-thaw cycles, representing a pivotal factor in assessing the freeze-thaw resistance of foamed concrete. The compressive strength loss rate was calculated by Eq. (1) (JGJ-T341-2014).

$$f_s = \frac{f_0 - f_n}{f_0} \times 100 \quad (1)$$

Where: f_s = the strength loss rate of specimens after freeze-thaw cycles, %; f_0 = the strength of specimens after 28-day standard curing, MPa; f_n = the strength of specimens after n freeze-thaw cycles, MPa.

The test results depicting the compressive strength and compressive strength loss rate of specimens subjected to different freeze-thaw cycles are illustrated in Fig. 3 With an increase in the number of freeze-thaw cycles, a consistent decline in compressive strength is observed. Starting at an initial strength (f_0) of 1.50 MPa, the specimen experiences a 16% decrease after 50 cycles, resulting in a strength of 1.26 MPa. Subsequently, after 300 freeze-thaw cycles, the compressive strength further decreases to 0.99 MPa, accounting for 66% of f_0. These findings parallel those reported by Tan *et al*. (2013), indicating a similar correlation between the reduction in sample strength and the number of freeze-thaw cycles.

In general, the freeze-thaw cycle test is stopped once the strength loss rate (f_s) surpasses 20% (JGJ-T341-2014). Observations indicate that upon reaching 100 freeze-thaw cycles, f_s exceeds 20%; however, the sample retains its structural integrity admirably. In the simulated testing environment, foamed concrete utilized for roadbed filling demonstrates an ability to meet strength criteria for a projected 60-year period.

The damage progression of the specimen following 0, 10, 50, 150, 200, and 300 freeze-thaw cycles is illustrated in Fig. 4. Initially, depicted in (a), (b), and (c) of Fig. 4, a discernible increase in the degree of spalling (the white circular area) and damage of the specimen's surface and corners accompanies a rise in freeze-thaw cycles. This deterioration can be attributed to several mechanisms,

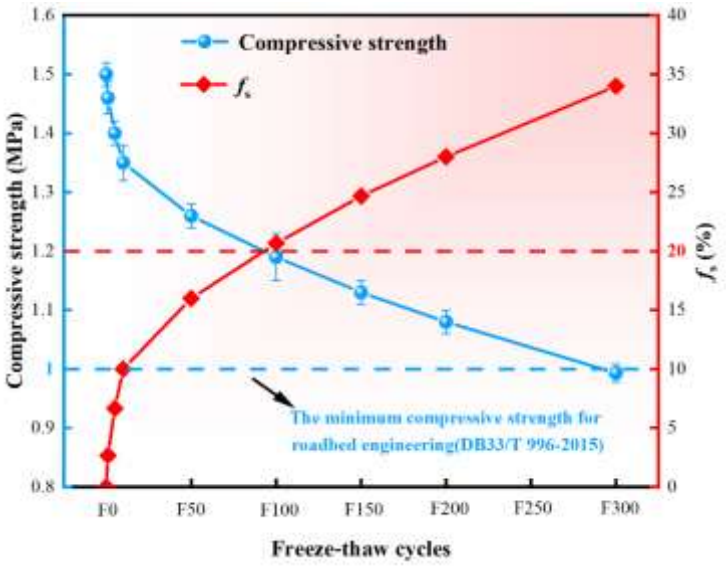

Fig. 3 Compressive strength and f_s of samples under freeze-thaw cycles

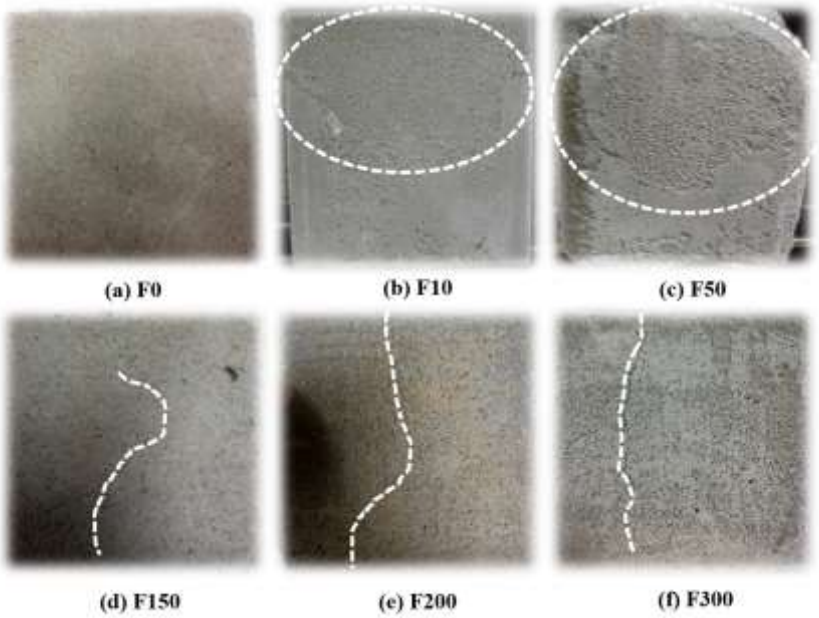

Fig. 4 Surface morphology of foamed concrete specimens after different freeze–thaw cycles

including hydraulic pressure induced by the volumetric expansion of water, crystallization pressure, and thermal mismatch between ice and the solid skeleton (Liu, *et al*. 2013). Among these, crystallization pressure is generally regarded as the dominant factor. When the temperature falls below 0°C, the water within the pores of saturated specimens undergoes freezing, leading to the formation of ice crystals within the pores. The growth of ice crystals imposes internal loads on the surrounding solid skeleton (Liu *et al*. 2013), resulting in local stress concentration, cavity damage, and the initiation of microcracks. These growing ice crystals exert frost pressure on the pore walls (Fan and Tian 2014, Zhang *et al*. 2018). If this pressure surpasses the permissible value for the foamed concrete pore wall, it results in the destruction of the pore structure within the foamed concrete, leading to the formation of numerous micro-cracks within the specimen. These micro-cracks facilitate increased water ingress (Richardson *et al*. 2012), escalating moisture content and internal micro-cracking, thereby exacerbating foamed concrete deterioration, and precipitating a notable decline in compressive strength. After more than 150 freeze-thaw cycles, visible cracks (the white dotted line) appear on the sample surface, as depicted in (d), (e), and (f) in Fig. 4. With an increasing number of freeze-thaw cycles, these cracks progressively propagate throughout the entire sample. Despite this, the sample retains its structural integrity.

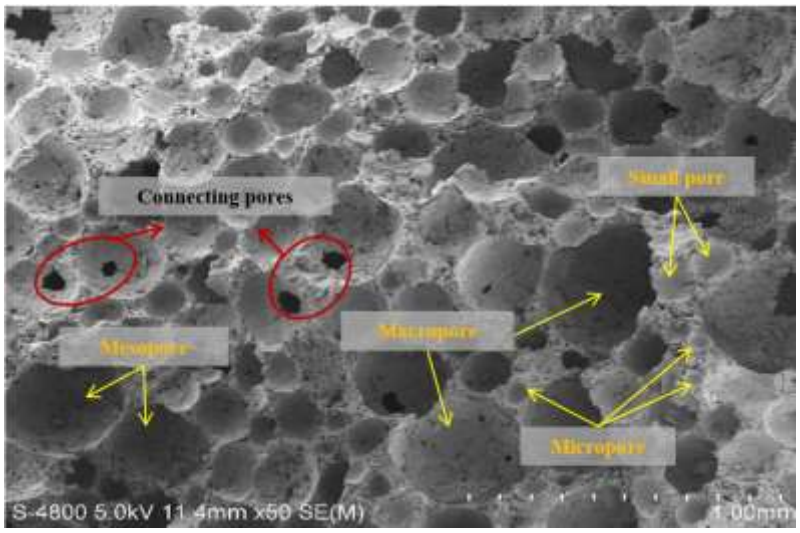

Fig. 5 SEM images of the prepared foamed concrete

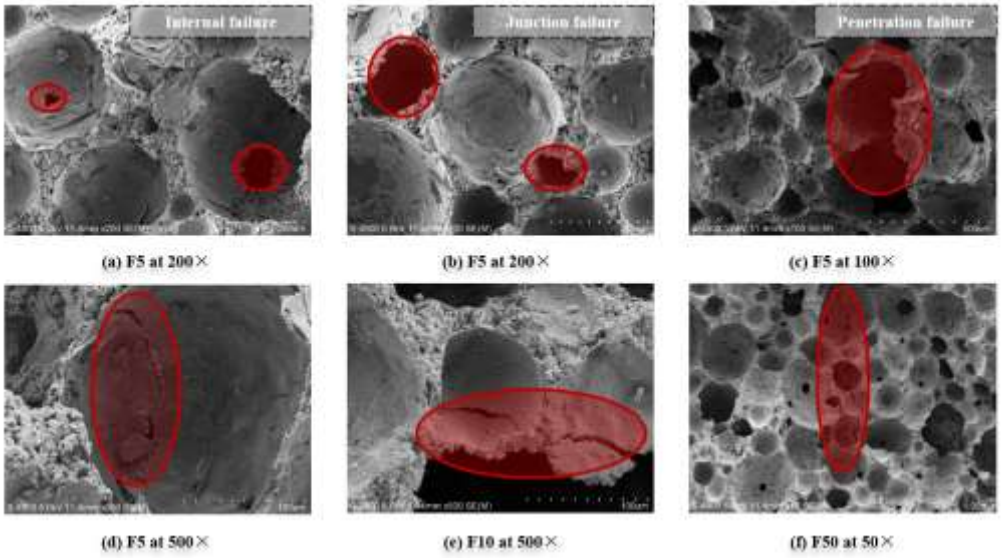

Fig. 6 SEM images of the foamed concrete after freeze-thaw cycles

3.2 Microstructural morphology of foamed concrete

The microstructure of foamed concrete before and after the freeze-thaw cycle is depicted in Figs. 5 and 6, respectively. Fig. 5 reveals a porous and uneven structure of the foamed concrete, particularly visible at 50 times magnification. Pores are observed in varying sizes, categorized roughly as macropores, mesopores, small pores, and micropores (Song *et al*. 2021), along with interconnected pores within the specimen. These features contribute to the reduced capacity and compressive strength of foamed concrete compared to ordinary concrete (Kearsley and Wainwright 2001).

According to the observed failure modes, the internal structural failure induced by freeze-thaw cycles can be categorized into cavity failure and crack failure. Based on the location and extent of failure, cavity failure can be further classified into internal failure (refer to Fig. 6(a)), junction failure (refer to Fig. 6(b)), and penetration failure (refer to Fig. 6(c)). When the temperature decreases, water within the cavities freezes and expands, generating frost-heaving pressure (Liu *et al*. 2011). This pressure produces stress concentrations on the cavity walls and their junctions, which weaken these regions and make them prone to damage. Consequently, failure may occur inside a single cavity (internal failure) or at the connections between adjacent cavities (junction failure). Concurrent internal and junction failures often escalate into penetration failure, wherein multiple cavities become interconnected, amplifying porosity and markedly diminishing specimen strength. At the same time, the tensile stress induced during frost heaving triggers internal crack propagation within foamed concrete, leading to crack failure categorized into initial stage (refer to Fig. 6(d)), intermediate stage (refer to Fig. 6(e)), and advanced stage (refer to Fig. 6(f)) based on progressive crack expansion phases. During the initial crack

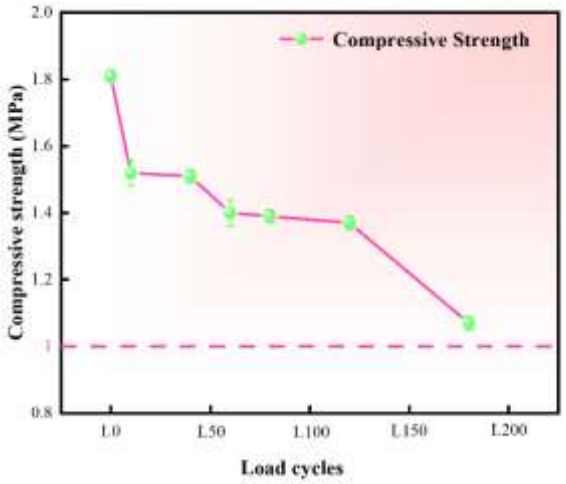

Fig. 7 Compressive strength of samples under load cycles

failure phase, tensile forces cause initial micro-cracks within the foamed concrete's internal cavities. With continued freeze-thaw cycles, these micro-cracks extend bidirectionally from a single cavity, bridging across interconnected pores due to recurring tensile stresses. Eventually, these micro-cracks traverse multiple adjacent cavities, forming larger penetrating cracks. Fig. 6(f) vividly illustrates such penetrating cracks at 50-fold magnification after 50 freeze-thaw cycles.

3.3 Load cycle test

The compressive strength test results for specimens subjected to various load cycles are presented in Fig. 7. The compressive strength of foamed concrete specimens decreases as the number of load cycles increases, and the curve can be roughly divided into three phases: a significant decrease in compressive strength occurs within the first 100,000 load cycles; followed by a gradual decline in strength between 100,000 and 1.2 million cycles. Beyond 1.2 million cycles, the foamed concrete specimen's strength experiences a notable decrease with increasing load cycles, reaching 1.07 MPa after 1.8 million cycles, representing 60% of its initial strength before the load cycle.

This is because the development of internal micro-cracks and damage of foamed concrete under cyclic load can be divided into three corresponding stages. The first stage is the formation stage of micro-cracks inside the foamed concrete. Due to the existence of weak areas inside the foamed concrete, in this stage, with the increase of load repetition times, a large number of micro-cracks quickly occur in the initial internal damage (that is, internal damage that may be caused by sampling, such as internal holes and micro-cracks) and the weak areas inside the cement mortar, which is manifested in the first few weeks of load cycle (10^4 cycles per week). The compressive strength of foamed concrete decreases rapidly, but with the further increase of the number of load cycles, the number of new cracks formed by weekly load cycles gradually decreases, and the process of forming micro-cracks in the weak areas of foamed concrete has been nearly completed. Due to the constraints of other aggregates, these formed micro-cracks cannot develop rapidly, and the strength decline rate of foamed concrete is gradually reduced. The fatigue process of foamed concrete progresses into its second stage, constituting the majority of its fatigue life, once the formation of micro-cracks in stress-concentrated weak areas is essentially completed. During this stage, the established cracks undergo stable expansion as cumulative damage accumulates, resulting in a continuous decrease in the fracture toughness of the cement mortar. Upon reaching a critical degree of damage, these micro-cracks transition to an unstable expansion phase, marking the onset of the third stage characterized by rapid fatigue damage escalation. This phase is distinguished by a sharp decrease in ultrasonic propagation speed and amplitude within the foamed concrete, leading to a pronounced decline in compressive strength. Notably, visible cracks emerge on the specimen surface at this juncture.

The load cycle test results indicate that under simulated conditions, the utilization of foamed concrete for roadbed filling satisfactorily meets the criteria for a 60-year highway service life. This underscores the foamed concrete's robust capacity to withstand vehicle loads.

3.4 Coupling cycle test

Fig. 8 depicts the damage conditions of 5 sample groups subjected to load cycles. Following 5 freeze-thaw cycles and 30,000 load cycles, sample F5L3 exhibited no discernible damage. During this period, the freeze-thaw environment and cyclic loading conditions did not compromise the specimen's integrity, maintaining its robust load-bearing capacity. Upon reaching 50 freeze-thaw cycles, sample F50L30 underwent cyclic loading and unloading. At approximately 120,000 cycles, visible micro-cracks (the white dotted line) emerged along the specimen's edge. Subsequently, these micro-cracks expanded gradually but did not result in specimen damage. A similar trend was observed in sample F100L60 and sample F50L30, where

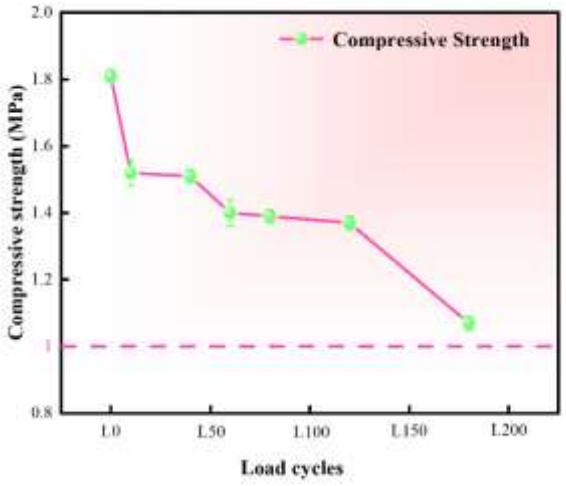

Fig. 7 Compressive strength of samples under load cycles

Fig. 8 Surface morphology of foamed concrete under cyclic loading

micro-cracks appeared at the edge after 80,000 cycles of cyclic loading and unloading. Although these micro-cracks expanded faster and wider than in sample F50L30, the specimens remained undamaged even after 600,000 cycles of loading and unloading. The sample F200L120, after undergoing 200 freeze-thaw cycles, was subjected to cyclic loading and unloading. At around 70,000 cycles of loading and unloading, cracks began to appear at the specimen's edge. This early initiation of cracks is primarily attributed to stress concentration and cumulative fatigue damage at the edges, where boundary effects and geometric discontinuities result in higher local tensile stresses (Liu *et al*. 2011). The prior 200 freeze–thaw cycles further weakened the microstructure, causing micro-defects in these regions to accumulate damage earlier than in the interior, thereby accelerating crack initiation. These cracks continued to expand and propagate with increasing cycles. In contrast to the three aforementioned simulation environments, the cracks in this specimen expanded diagonally by about 45°. However, despite the completion of cyclic loading and unloading, the specimen remained intact and retained a certain level of strength. Sample F300L180 underwent simulation for 300 freeze-thaw cycles and 1.8 million cycles of loading and unloading. After the completion of 300 freeze-thaw cycles, cyclic loading and unloading were initiated. At around 50,000 cycles, micro-cracks became visible on the specimen's surface, rapidly expanding as the cycles progressed. By the time the cycles reached approximately 100,000, the micro-cracks had penetrated the entire specimen, leading to its failure and preventing the subsequent unconfined compressive strength test.

Unconfined compressive strength tests were conducted on the four groups of samples (F5L3~F200L120) that remained undamaged following the freeze-thaw and load cycles. The test results are shown in Fig. 9. The strength loss rate was calculated to quantify the internal damage of the specimens. As the service life of foamed concrete increases, its internal structure becomes compromised, leading to a notable decline in compressive strength and the accumulation of internal damage. At the 10-year mark, the compressive strength of foamed concrete decreases to 0.96 MPa, with an accompanying strength loss rate of 20.66%. Consequently, the foamed concrete fails to meet the strength specifications for roadbed engineering (>1.0 MPa). Initially, the compressive strength of foamed concrete samples decreases rapidly with an increase in freeze-thaw and load cycles. However, as the simulated service life surpasses 20 years, the rate of decline in compressive strength begins to decelerate. For instance, in comparison to the F200L120 sample, the compressive strength of the F100L60 sample decreased by only 0.05 MPa.

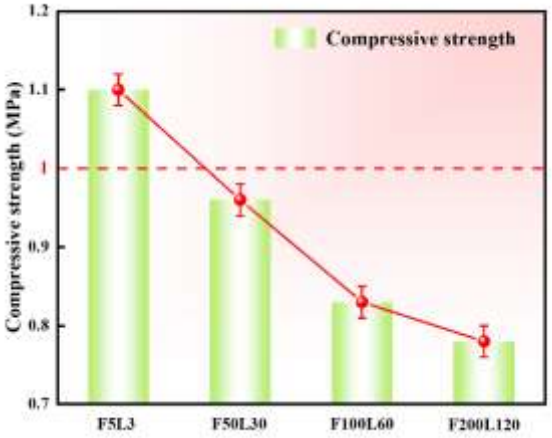

Fig. 9 Compressive strength of samples after coupling cycles

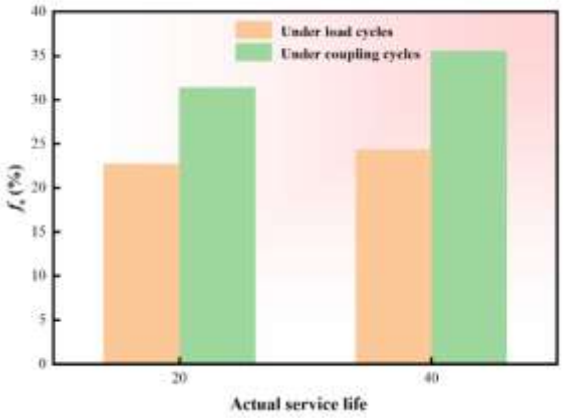

Fig. 10 Compressive strength loss rate under load cycles and coupling cycles

This is because there are weak areas and main bearing areas in the internal structure of foamed concrete, and the weak area refers to the cement and coarse aggregate bond and hole connections; The main bearing area is the solid skeleton. Weak areas within the foamed concrete's structure are susceptible to early damage and destruction under cyclic loading, whereas the main bearing area undergoes gradual deterioration in response to such loading conditions.

At the same time, the impact of freeze-thaw cycles on the compressive strength of specimens is noteworthy. Fig. 10 illustrates the strength loss of specimens under various service life conditions in both load cycle and coupling cycle simulation environments. Observably, freeze-thaw cycles exacerbate strength loss and compromise specimen durability. For instance, after 20 years of service, f_s was 22.7% in the load cycle simulation environment and 31.4% in the coupling cycle simulation environment. During freeze-thaw cycles, the compressive strength loss of foamed concrete primarily hinges on its pore structure and porosity (Gong and Zhang 2019). At lower temperatures, water within the foamed concrete's pores undergoes freeze force swelling, leading to micro-cracks formation. When the external force ranges from 0.1 f_c to 0.66 f_c, the exerted external pressure and the freeze force swelling engendered by internal water impact the internal structure, resulting in secondary cracks in the foamed concrete (Dry 2000, Matallah *et al*. 2010, Qi *et al*. 2003). Once these cracks reach a critical extent, water molecules infiltrate the specimen through them, inducing further damage. Concurrently, the cement binder's water absorption capacity diminishes (Zhang *et al*. 2024). Consequently, the compressive strength loss of foamed concrete specimens significantly escalates compared to those unaffected by freeze-thaw cycles.

4. Conclusions

This paper investigates the long-term durability of foamed concrete in highway engineering, considering the effects of freeze-thaw cycles, load cycles, and coupling cycles. The overall morphology and microscopic failure characteristics of foamed concrete under the freeze-thaw cycles are analyzed by scanning electron microscopy. The main conclusions of this study are as follows:

- The compressive strength of foamed concrete gradually declines as the number of freeze-thaw cycles increases. After 150 cycles (approximately

corresponding to 30 years after the opening of the highway), surface cracks become evident on the foamed concrete sample. Upon reaching 300 cycles (approximately corresponding to 60 years of the opening of the highway), the compressive strength decreases from 1.50 MPa to 0.99 MPa, marking a 34% reduction.

- SEM analysis reveals that internal structure failure induced by freeze-thaw cycles categorically manifests as cavity and crack failures. Cavity failure encompasses internal, junction, and penetration failures, arising from material contraction due to hydrostatic pressure triggered by frost heave. Crack failure, instigated by tensile stress, unfolds across the initial, middle, and advanced stages of crack propagation. Cracks progressively traverse multiple holes, culminating in the formation of larger penetration cracks, thereby substantially compromising specimen strength.
- Under the load cycle, with the increase of the load cycle, the degradation process of foamed concrete strength can be divided into three stages. Among them, the compressive strength attenuation is relatively slow in 100,000-1.2 million cycles. After 1.8 million load cycles—equivalent to approximately 60 years of highway service—the compressive strength of the specimen decreased to 1.07 MPa, representing about 60% of its initial strength prior to cyclic loading.
- Cracks manifest on the surface of foamed concrete samples to varying degrees under coupling cycles. As service life progresses, the compressive strength of foamed concrete markedly diminishes, while internal damage accrues incessantly. By the tenth year of service, foamed concrete's compressive strength reduces to 0.96 MPa, rendering it incapable of meeting the strength prerequisites for roadbed engineering (> 1.0 MPa).

This paper systematically investigates the durability of foamed concrete under freeze-thaw cycle, load cycle, and coupling cycle conditions, yielding promising results. Nonetheless, in real-world roadbed engineering applications, the environments encountered by foamed concrete are highly intricate. Hence, future research endeavors should prioritize exploring the durability of foamed concrete in various complex coupled environments and elucidating its strength evolution patterns. This endeavor aims to furnish a theoretical framework for enhancing the durability of foamed concrete, thereby facilitating its wider adoption in highway engineering.

Acknowledgments

Financial support from the National Natural Science Foundation of China (52178327) and the Postgraduate Research & Practice Innovation Program of Jiangsu Province (KYCX23_0699) are gratefully acknowledged.

References

Amran, M., Onaizi, A.M., Fediuk, R., Danish, A., Vatin, N.I., Murali, G., Abdelgader, H.S., Mosaberpanah, M.A., Cecchin, D. and Azevedo, A. (2022), "An ultra-lightweight cellular concrete for geotechnical applications-A review", *Case Stud. Constr. Mater.*, **16**, e01096. https://doi.org/10.1016/j.cscm.2022.e01096.

Amran, Y.H.M., Farzadnia, N. and Abang Ali, A.A. (2015), "Properties and applications of foamed concrete; A review", *Constr. Build. Mater.*, **101**, 990-1005. https://doi.org/10.1016/j.conbuildmat.2015.10.112.

Arasan, S. and Nasirpur, O. (2015), "The effects of polymers and fly ash on unconfined compressive strength and freeze-thaw behavior of loose saturated sand", *Geomech. Eng.*, **8**(3), 361-375. https://doi.org/10.12989/gae.2015.8.3.361.

ASTM C 666-97 (2015), *Standard Test Method for Resistance of Concrete to Rapid Freezing and Thawing*, ASTM International; USA.

Brown, S.F. (1996), "Soil mechanics in pavement engineering", *Geotechnique*, **46**(3), 383-425. https://doi.org/10.1680/geot.1996.46.3.383.

Cai, D.G., Wei, S.W., Ye, Y.S., Zhang, Q.L., Li, Z.G. and Li, S. (2021), "Mechanical properties of lightweight foam concrete filler for roadbed of high-speed railway", *Arab. J. Geosci.*, **14**(10), 902. https://doi.org/10.1007/s12517-021-07115-1.

Chai, J.C. and Miura, N. (2002), "Traffic-load-induced permanent deformation of road on soft subsoil", *J. Geotech. Geoenviron. Eng.*, **128**(11), 907-916. https://doi.org/10.1061/(ASCE)1090-0241(2002)128:11(907).

Chandni, T.J. and Anand, K.B. (2018), "Utilization of recycled waste as filler in foam concrete", *J. Build. Eng.*, **19**, 154-160. https://doi.org/10.1016/j.jobe.2018.04.032.

Cheng, S.K., Wang, Q., Fu, H.C., Wang, J.Q., Han, Y., Shen, J.J. and Lin, S. (2021), "Effect of freeze-thaw cycles on the mechanical properties and constitutive model of saline soil", *Geomech. Eng.*, **27**(4), 309-322. https://doi.org/10.12989/gae.2021.27.4.309.

Cui, X., Du, Y., Bao, Z., Xiao, Y., Hao, J., Li, X. and Zhang, S. (2023), "Field evaluation of the three-dimensional dynamic stress state of the subgrade induced by the heavy-haul train load", *Transp. Geotech.*, **38**, 100903. https://doi.org/10.1016/j.trgeo.2022.100903.

DB33/T 996-2015 (2015), *Technical Specification for Foamed Concrete Application on Highway*, Ministry of Housing and Urban-Rural Construction of the People's Republic of China; Beijing, China.

Dry, C.M. (2000), "Three designs for the internal release of sealants, adhesives, and waterproofing chemicals into concrete to reduce permeability", *Cem. Concr. Res.*, 30(12), 1969-1977. https://doi.org/10.1016/S0008-8846(00)00415-4.

Fan, C.X. and Tian, H. (2013), "Advances in damage of concrete due to freeze-thaw circles", *Proc., 3rd International Conference on Civil Engineering and Transportation, ICCET 2013, December 14, 2013 - December 15, 2013*, Trans Tech Publications Ltd, 204-208.

Feng, S., Zhou, Y., Wang, Y. and Lei, M. (2020), "Experimental research on the dynamic mechanical properties and damage characteristics of lightweight foamed concrete under impact loading", *Int. J. Impact Eng.*, **140**, 103558. https://doi.org/10.1016/j.ijimpeng.2020.103558.

GB/T 17671-2021 (2021), *Test method of cement mortar strength*, Ministry of Housing and Urban-Rural Construction of the People's Republic of China; Beijing, China.

GB/T 50082–2009 (2009), *Standard for test methods of long-term performance and durability of ordinary concrete*, Ministry of Housing and Urban-Rural Construction of the People's Republic of China; Beijing, China.

Gong, J. and Zhang, W. (2019), "The effects of pozzolanic powder on foam concrete pore structure and frost resistance", *Constr. Build. Mater.*, **208**, 135-143. https://doi.org/10.1016/j.conbuildmat.2019.02.021.

JGJ-T341-2014 (2014), *Technical code for application of foamed concrete*, Ministry of Housing and Urban-Rural Construction of the People's Republic of China; Beijing, China.

JG/T 266-2011 (2011), *Foamed concrete*, Ministry of Housing and Urban-Rural Construction of the People's Republic of China; Beijing, China.

Jones, M. and McCarthy, A. (2005), "Utilising unprocessed low-lime coal fly ash in foamed concrete", *Fuel*, **84**(11), 1398-1409. http://dx.doi.org/10.1016/j.fuel.2004.09.030.

JTG B01-2014 (2014), *Technical Standard of Highway Engineering*, Ministry of Housing and Urban-Rural Construction of the People's Republic of China; Beijing, China.

Kadela, M. and Kozlowski, M. (2016), "Foamed concrete layer as sub-structure of industrial concrete floor", *Proceedings of the World Multidisciplinary Civil Engineering-Architecture-Urban Planning Symposium (WMCAUS)*, 468-476.

Kearsley, E.P. and Wainwright, P.J. (2001), "Porosity and permeability of foamed concrete", *Cement Concrete Res.*, **31**(5), 805-812. https://doi.org/10.1016/s0008-8846(01)00490-2.

Kilincarslan, S., Davraz, M. and Akça, M. (2018),. "The effect of pumice as aggregate on the mechanical and thermal properties of foam concrete", *Arab. J. Geosci.*, **11**(11), 289. https://doi.org/10.1007/s12517-018-3627-y.

Kim, T.H., Kim, T.H. and Kang, G.C. (2013), "Performance evaluation of road embankment constructed using lightweight soils on an unimproved soft soil layer", *Eng. Geol.*, **160**, 34-43. https://doi.org/10.1016/j.enggeo.2013.03.024.

Krechowiecki-Shaw, C.J., Jefferson, I., Royal, A., Ghataora, G.S. and Alobaidi, I.M. (2016), "Degradation of soft subgrade soil from slow, large, cyclic heavy-haul road loads: a review", *Can. Geotech. J.*, **53**(9), 1435-1449. https://doi.org/10.1139/cgj-2015-0234.

Li, J., Peng, X., Deng, Z., Cao, J., Guan, Y. and Lin, L. (2000), "Quantitative design on the frost-resistance of concrete", *Concrete*, **12**(134) [In Chinese].

Li, J., Sun, Z., Pang, M., Tian, J., Ling, Y., Luo, S. and Li, F. (2020), "Study on preparation and durability of phosphogypsum composite cementitious foam concrete", *J. Phys.: Conference Series*, **1646**(1), 012102.

Liu, L., Chen, H., Sun, W. and Ye, G. (2013), "Microstructure-based modeling of the diffusivity of cement paste with micro-cracks", *Constr. Build. Mater.*, **38**, 1107-1116. https://doi.org/10.1016/j.conbuildmat.2012.10.002.

Liu, L., Ye, G., Schlangen, E., Chen, H., Qian, Z., Sun, W. and van Breugel, K. (2011). "Modeling of the internal damage of saturated cement paste due to ice crystallization pressure during freezing", *Cement Concrete Compos.*, **33**(5), 562-571. https://doi.org/10.1016/j.cemconcomp.2011.03.001.

Lu, Z., Fang, R., Yao, H., Hu, Z. and Liu, J. (2018). "Evaluation and analysis of the traffic load–induced settlement of roads on soft subsoils with low embankments", *Int. J. Geomech.*, **18**(6), 04018043. https://doi.org/10.1061/(ASCE)GM.1943-5622.0001123.

Matallah, M., La Borderie, C. and Maurel, O. (2010), "A practical method to estimate crack openings in concrete structures", *Int. J. Numer. Anal. Method. Geomech.*, **34**(15), 1615-1633. https://doi.org/10.1002/nag.876.

Qi, C., Weiss, J. and Olek, J. (2003), "Characterization of plastic shrinkage cracking in fiber reinforced concrete using image analysis and a modified Weibull function", *Mater. Struct.*, **36**(6), 386-395. https://doi.org/10.1007/BF02481064.

Rahgooy, K., Bahmanpour, A., Derakhshandi, M. and Bagherzadeh-Khalkhali, A. (2022), "Distribution of elastoplastic modulus of subgrade reaction for analysis of raft foundations", *Geomech. Eng.*, **28**(1), 89-105. https://doi.org/10.12989/gae.2022.28.1.089.

Raj, A., Sathyan, D. and Mini, K.M. (2021), "Performance evaluation of natural fiber reinforced high volume fly ash foam concrete cladding", *Adv. Concrete. Constr.*, **11**, 151-161. https://doi.org/10.12989/acc.2021.11.2.151.

Ramamurthy, K., Nambiar, E.K.K. and Ranjani, G.I.S. (2009), "A classification of studies on properties of foam concrete", *Cement Concrete Compos.*, **31**(6), 388-396. http://dx.doi.org/10.1016/j.cemconcomp.2009.04.006.

Richardson, A.E., Coventry, K.A. and Wilkinson, S. (2012), "Freeze/thaw durability of concrete with synthetic fibre additions", *Cold Reg. Sci. Technol.*, **83-84**, 49-56. http://dx.doi.org/10.1016/j.coldregions.2012.06.006.

She, W., Du, Y., Zhao, G., Feng, P., Zhang, Y. and Cao, X. (2018), "Influence of coarse fly ash on the performance of foam concrete and its application in high-speed railway roadbeds", *Constr. Build. Mater.*, **170**, 153-166. http://dx.doi.org/10.1016/j.conbuildmat.2018.02.207.

Shi, X., Huang, J. and Su, Q. (2020), "Experimental and numerical analyses of lightweight foamed concrete as filler for widening embankment", *Constr. Build. Mater.*, **250**, 118897. http://dx.doi.org/10.1016/j.conbuildmat.2020.118897.

Song, Q., Bao, J., Xue, S., Zhang, P. and Mu, S. (2021), "Collaborative disposal of multisource solid waste: Influence of an admixture on the properties, pore structure and durability of foam concrete", *J. Mater. Res. Technol-JMRT*, **14**, 1778-1790. http://dx.doi.org/10.1016/j.jmrt.2021.07.075.

Steyn, W. J., Lombard, S. and Horak, E. (2016), "Foamed concrete-based material as a soft ground arresting system for runways and airfields", *J. Perform. Constr. Fac.*, **30**(1), C4014006. https://doi.org/10.1061/(asce)cf.1943-5509.0000692.

Tan, X., Chen, W., Tian, H. and Yuan, J. (2013), "Degradation characteristics of foamed concrete with lightweight aggregate and polypropylene fibre under freeze-thaw cycles", *Mag. Concrete Res.*, **65**(12), 720-730. https://doi.org/10.1680/macr.12.00145.

Tang, L.S., Chen, H.K., Sun, Y.L., Zhang, Q.H. and Liao, H.R. (2018), "Traffic-load-induced dynamic stress accumulation in subgrade and subsoil using small scale model tests", *Geomech. Eng.*, **16**(2), 113-124. https://doi.org/10.12989/gae.2018.16.2.113.

Tang, R., Wei, Q., Zhang, K., Jiang, S., Shen, Z., Zhang, Y. and Chow, C.W.K. (2022), "Preparation and performance analysis of recycled PET fiber reinforced recycled foamed concrete", *J. Build. Eng.*, **57**, 104948. https://doi.org/10.1016/j.jobe.2022.104948.

Tikalsky, P.J., Pospisil, J. and MacDonald, W. (2004), "A method for assessment of the freeze-thaw resistance of preformed foam cellular concrete", *Cement Concrete Res.*, **34**(5), 889-893. https://doi.org/10.1016/j.cemconres.2003.11.005.

Van Dijk, S. (1991), *Foamed concrete: a dutch view*, British Cement Association; British.

Wang, W., Zhong, Z., Kang, X. and Ma, X. (2023), "Physico-mechanical properties and micromorphological characteristics of graphene oxide reinforced geopolymer foam concrete", *J. Build. Eng.*, **72**, 106732. https://doi.org/10.1016/j.jobe.2023.106732.

Wei, S., Chen, Y.Q., Zhang, Y.S. and M.R., J. (2013), "Characterization and simulation of microstructure and thermal properties of foamed concrete", *Constr. Build. Mater.*, **47**, 1278-1291. http://dx.doi.org/10.1016/j.conbuildmat.2013.06.027.

Wei, X., Ding, Y. and Li, X. (2012), "Review and prospect of freeze-thaw-induced erosion research", *Res. Soil Water Conserv.*, **19**(2), 271-275.

Wu, G., Xie, Y., Wei, J. and Yue, X. (2023), "Freeze-thaw erosion

mechanism and preventive actions of highway subgrade soil in an alpine meadow on the Qinghai-Tibet Plateau", *Eng. Fail. Anal.*, **143**, 106933. https://doi.org/10.1016/j.engfailanal.2022.106933.

Wu, J., Wang, J., Liu, M., Zhuang, P., Zhang, H. and Song, X. (2022), "Dynamic properties of silt-based foamed concrete as filler in subgrade", *J. Mater. Civ. Eng.*, **34**(10), 04022241. https://doi.org/10.1061/(ASCE)MT.1943-5533.0004398.

Xu, Z., Chen, Z. and Yang, S. (2018), "Effect of a new type of high-strength lightweight foamed concrete on seismic performance of cold-formed steel shear walls", *Constr. Build. Mater.*, **181**, 287-300. https://doi.org/10.1016/j.conbuildmat.2018.06.067.

Zhang, H., Qi, X., Wan, L., Zuo, Z., Ge, Z., Wu, J. and Song, X. (2020). "Properties of silt-based foamed concrete: A type of material for use in backfill behind an abutment", *Constr. Build. Mater.*, **261**, 119966. http://dx.doi.org/10.1016/j.conbuildmat.2020.119966.

Zhang, H., Wang, J., Liu, Z., Ma, C., Song, Z., Cui, F., Wu, J. and Song, X. (2024), "Strength characteristics of foamed concrete under coupling effect of constant compressive loading and freeze-thaw cycles", *Constr. Build. Mater.*, **411**, 134565. http://dx.doi.org/10.1016/j.conbuildmat.2023.134565.

Zhang, H., Wang, J., Wang, C., Liu, M. and Wu, J. (2023), "Using foamed concrete layer to optimize the design of pPavement and subgrade structures: From the perspectives economy and durability", *Arab. J. Sci. Eng.*, **48**(10), 12859-12874. http://dx.doi.org/10.1007/s13369-023-07606-1.

Zhang, P., Dai, Y., Ding, X., Zhou, C., Xue, X. and Zhao, T. (2018), "Self-healing behaviour of multiple microcracks of strain hardening cementitious composites (SHCC)", *Constr. Build. Mater.*, **169**, 705-715. http://dx.doi.org/10.1016/j.conbuildmat.2018.03.032.

Zhang, S., Liu, M., Wang, C., Zhang, H. and Wu, J. (2022). "Compression, Unloading-reloading, and tension mechanical behaviors of Silt-based foamed concrete under uniaxial loading", *Constr. Build. Mater.*, **347**, 128558. https://doi.org/10.1016/j.conbuildmat.2022.128558.

Zhong, D., Wang, S., Gao, Y., Wang, L. and Feng, K. (2021), "Experimental study on freeze-thaw resistance of modified magnesium oxychloride cement foam concrete", *J. Phys.: Conference Series*, **1885**(3), 032009.